Yeast AMP-activated protein kinase monitors glucose concentration changes and absolute glucose levels

THE JOURNAL OF BIOLOGICAL CHEMISTRY VOL. 289, NO. 18, pp. 12863–12875, May 2, 2014

Yeast AMP-activated Protein Kinase Monitors Glucose Concentration Changes and Absolute Glucose Levels*

Received for publication, January 9, 2014, and in revised form, March 4, 2014 Published, JBC Papers in Press, March 13, 2014, DOI 10.1074/jbc.M114.547976

Loubna Bendrioua[‡], Maria Smedh[§], Joachim Almquist[¶‖], Marija Cvijovic[**], Mats Jirstrand[¶], Mattias Goksör[‡‡], Caroline B. Adiels[‡‡], and Stefan Hohmann[‡1]

From the [‡]Department of Chemistry and Molecular Biology, University of Gothenburg, 40530 Göteborg, Sweden, the [§]Centre for Cellular Imaging, Sahlgrenska Core Facilities, University of Gothenburg, 40530 Göteborg, Sweden, [¶]Systems and Data Analysis, Fraunhofer-Chalmers Research Centre Industrial Mathematics, 41288 Göteborg, Sweden, [‖]Systems and Synthetic Biology, Department of Chemical and Biological Engineering, Chalmers University of Technology, 41296 Göteborg, Sweden, the [**]Department of Mathematical Sciences, Chalmers University of Technology and University of Gothenburg, 41296 Göteborg, Sweden, and the [‡‡]Department of Physics, University of Gothenburg, 41296 Göteborg, Sweden

Background: Little is known about the signaling dynamics of AMP-activated protein kinase.
Results: We define the dynamics of yeast AMPK signaling under different glucose concentrations.
Conclusion: The Snf1-Mig1 signaling system monitors glucose concentration changes and absolute glucose levels to adjust the metabolism to a wide range of conditions.
Significance: This description of AMPK signaling dynamics will stimulate studies defining the integration of signaling and metabolism.

Analysis of the time-dependent behavior of a signaling system can provide insight into its dynamic properties. We employed the nucleocytoplasmic shuttling of the transcriptional repressor Mig1 as readout to characterize Snf1-Mig1 dynamics in single yeast cells. Mig1 binds to promoters of target genes and mediates glucose repression. Mig1 is predominantly located in the nucleus when glucose is abundant. Upon glucose depletion, Mig1 is phosphorylated by the yeast AMP-activated kinase Snf1 and exported into the cytoplasm. We used a three-channel microfluidic device to establish a high degree of control over the glucose concentration exposed to cells. Following regimes of glucose up- and downshifts, we observed a very rapid response reaching a new steady state within less than 1 min, different glucose threshold concentrations depending on glucose up- or downshifts, a graded profile with increased cell-to-cell variation at threshold glucose concentrations, and biphasic behavior with a transient translocation of Mig1 upon the shift from high to intermediate glucose concentrations. Fluorescence loss in photobleaching and fluorescence recovery after photobleaching data demonstrate that Mig1 shuttles constantly between the nucleus and cytoplasm, although with different rates, depending on the presence of glucose. Taken together, our data suggest that the Snf1-Mig1 system has the ability to monitor glucose concentration changes as well as absolute glucose levels. The sensitivity over a wide range of glucose levels and different glucose concentration-dependent response profiles are likely determined by the close integration of signaling with the metabolism and may provide for a highly flexible and fast adaptation to an altered nutritional status.

Signal transduction progresses through a series of transient protein-protein interactions and protein modifications to transmit the signal from the site of sensing to where the response is triggered. Understanding the mechanisms that control the dynamics of signal transmission requires measurements that capture the underlying processes as closely as possible in real time. Following signal transmission in real time is possible in living cells using imaging in well controlled microfluidic chambers and appropriate reporters/readouts. Changes in the subcellular localization of signaling proteins as a consequence of signal progression offer the opportunity to observe signaling as it occurs. In the yeast *Saccharomyces cerevisiae*, signaling has been monitored employing cytoplasmic-nuclear shuttling of protein kinases and transcription factors for the osmo-sensing High Osmolarity Glycerol (HOG) pathway (the Hog1 MAP kinase) (1–5), the calcineurin pathway (the Crz1 transcriptional activator) (6), the protein kinase A pathway (the Msn2 transcriptional activator) (7–9), and oxidative stress signaling through Yap1 (10). Several interesting system properties have been observed, including perfect adaptation of the Hog1 signaling system (1), slowdown of protein movements as a consequence of molecular crowding in compressed cells following osmostress (3, 5), the potential benefits of nuclear accumulation bursts to coordinate multigene responses to external signals or for the survival of cell populations (8, 9), and how coupling of dynamic phenomena may establish a rate of change sensor (7).

The adenosine monophosphate-activated kinase (AMPK)[2] is the master regulator of energy homeostasis in eukaryotic cells and is well conserved at the structural and physiological levels (13). AMPK appears to be controlled by multiple stimuli but most prominently by the cellular energy status via the levels of

* This work was supported by European Commission UNICELLSYS project contract 201142 (to S. H., M. G., and M. J.) and by ISOLATE project contract 289995 (to S. H. and M. G).

[1] To whom correspondence should be addressed: Dept. of Chemistry and Molecular Biology, University of Gothenburg, Box 462, 40530 Göteborg, Sweden. Tel.: 46-31-3608488; Fax: 46-31-7862599; E-mail: stefan.hohmann@gu.se.

[2] The abbreviations used are: AMPK, AMP-activated protein kinase; FRAP, fluorescence recovery after photobleaching; FLIP, fluorescence loss in photobleaching.

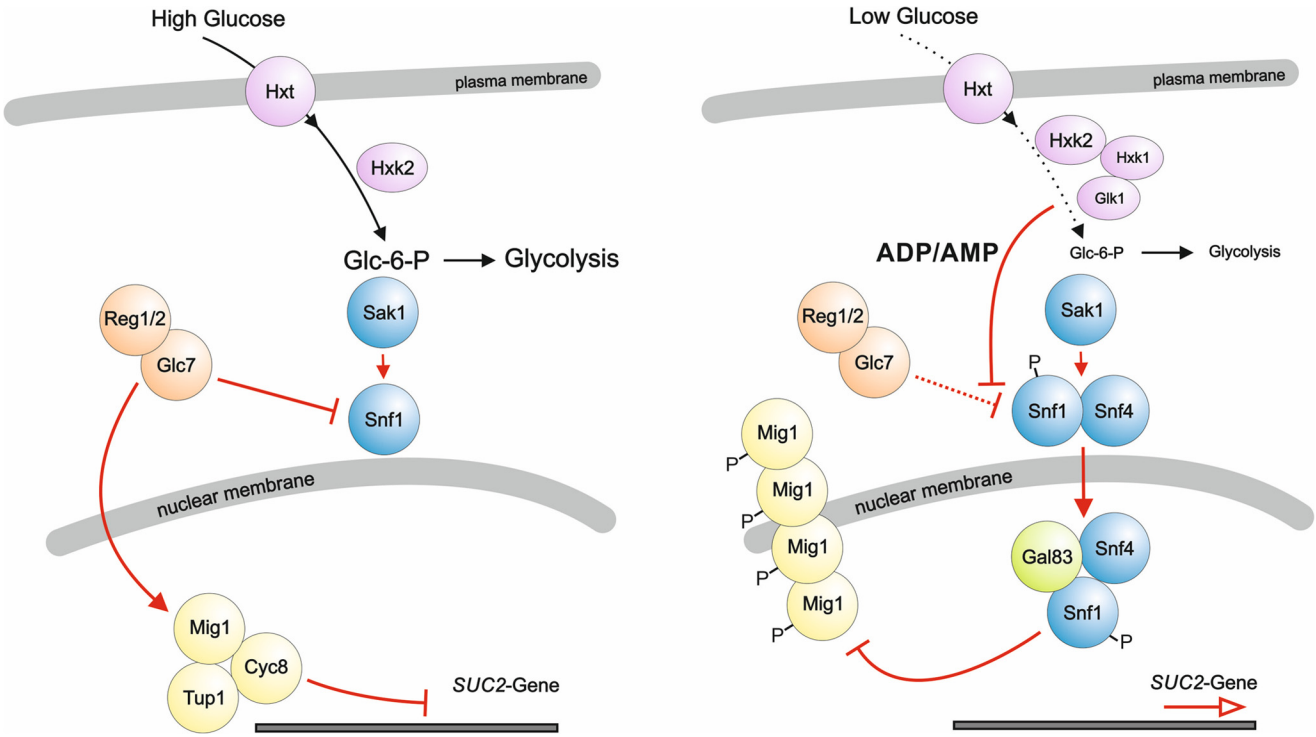

FIGURE 1. **Schematic representation of the yeast Snf1/Mig1 signaling pathway.** Shown is the Snf1/Mig1 pathway in the presence of high and low glucose levels in the growth medium. At high glucose levels, hexokinase PII (*Hxk2*) phosphorylates glucose, and glycolysis is fully active. The Glc7 phosphatase keeps Snf1 and Mig1 dephosphorylated, and, hence, Mig1 is located in the nucleus and, in complex with Cyc8 and Tup1, represses gene expression. At low glucose levels, hexokinase PI (*Hxk1*) and glucokinase (*Glk1*) also participate in glucose phosphorylation, but glycolysis is running at lower rate. ADP/AMP protect the SNF1 complex from dephosphorylation, and SNF1 phosphorylates Mig1, mediating its dissociation from Cyc8 and Tup1 and its nuclear exit. Snf1 is phosphorylated by three upstream kinases (*Sak1*, *Tos3*, and *Elm1*). Only Sak1 is shown. *Glc-6-P*, glucose 6-phosphate; *Hxt*, hexose transporter.

ATP, ADP, and AMP, and it stimulates ATP-producing processes and down-regulates ATP-consuming processes (11, 13–15). The sucrose non-fermenting (Snf1) protein kinase represents the yeast orthologue. Like mammalian AMPK, SNF1 (Fig. 1) is a complex consisting of three different subunits: the catalytic α subunit Snf1; the scaffolding and targeting alternative β subunits Sip1, Sip2, and Gal83; as well as the regulatory Snf4 subunit (11). Activation of Snf1 requires phosphorylation by any of three upstream kinases (Sak1, Tos3, and Elm1) and is negatively regulated by several protein phosphatases, most importantly Glc7-Reg1. Snf1 is best known for its role in the glucose derepression of genes whose products are required for the utilization of carbon sources other than glucose. In the presence of glucose, the multicopy inhibitor of *GAL* gene expression (Mig1), a Cys^2-His^2 zinc finger DNA binding protein, is poorly phosphorylated, located predominantly inside the nucleus, and blocks activity of numerous glucose-repressed promoters (reviewed in Refs. 11, 12, 16, 17). Mig1 recruits to those promoters the general repressor complex Cyc8-Tup1 (18–20) (Fig. 1). When glucose levels are low or glucose is completely absent, Snf1 is activated and phosphorylates Mig1 at multiple sites (21, 22). Phosphorylated Mig1 no longer interacts with Cyc8-Tup1 (23) and is translocated to the cytosol (24–26). Expression of the glucose-repressed genes is then stimulated by specific activation mechanisms (reviewed in Refs. 11, 12, 16). Readdition of glucose to such cells leads to rapid Mig1 dephosphorylation, followed by its accumulation in the nucleus (Ref. 26 and this work).

Hence, it appears that nuclear-cytosolic shuttling of Mig1 could serve as a real-time, or close to real-time, readout for the signaling behavior of the Snf1-Mig1 regulatory module. We decided to determine the threshold glucose concentrations for Mig1 nuclear/cytosolic accumulation following glucose up- and downshifts and to study the behavior of the signaling system around the glucose threshold. Thereby, we envisaged different possible behaviors around glucose thresholds, such as all or nothing *versus* graded responses, uniform behavior *versus* increased cell-to-cell variability, or even oscillations.

EXPERIMENTAL PROCEDURES

Yeast Strains—For microscopy experiments, we employed the YSH2348 strain (*MATa MIG1-GFP-HIS3 NRD1-mCherry-hphNT1 MET LYS*) in the BY4741 background. Yeast cells were grown to mid-log phase at 30 °C in synthetic complete medium containing 1.7 g/liter yeast nitrogen base, 5 g/liter ammonium sulfate, 670 mg/l complete supplement mix and supplied with 4% glucose or 3% ethanol. Serial dilutions of a 50% glucose stock solution in yeast nitrogen base were performed to generate glucose solutions ranging between 4–0.005%, corresponding to 220–0.275 mM glucose, respectively.

Microfluidics—To enable rapid changes of the glucose concentration around the cells, we used polydimethylsiloxane (Sylgard 184, Dow Corning, Seneffe, Belgium) custom-made microfluidic devices having three inlet channels that merge into one single channel of 410-μm width. The microfluidic device was manufactured as described previously (27). To attach cells

to the device surface, the microfluidic system was pretreated with 1 mg/ml of concanavalin A resuspended in 10 mM Tris-HCl and 100 mM NaCl (pH 8.0) for at least 30 min. The cell suspension was introduced into the lower inlet channel, whereas the middle channel contained the start growth medium, and the top inlet channel contained different glucose concentrations. Individual cells were trapped with optical tweezers and positioned in an array of 6 × 5 cells in a predefined measurement area so that all the cells were exposed to the same glucose concentration (28). The measurement area was identified on the basis of simulations using the software chemical engineering module of COMSOL MultiPhysics (COMSOL, Burlington, MA) (29).

The flow inside the channels was controlled by a set of syringe pumps (CMA Microdialysis AB, Sweden) monitored by custom-made automations using OpenLab (Improvision Inc.). The three inlets were connected to syringe pumps via polytetrafluoroethylene tubing (Cole-Parmer, Vernon Hills, IL), and needles were connected to 250-μl Hamilton glass syringes (Hamilton Co.). Both the lower and the middle inlet were connected to the same pump (pump I), whereas the upper inlet was connected to a second pump (pump II). At the start of the experiment, pump I was set to 80 nl/min, and pump II was set to 40 nl/min. To shift to test medium, pump I was turned off, whereas pump II was switched to 1000 nl/min. The flow changes and image acquisition events were synchronized by the OpenLab Automator extension of the OpenLab software.

Microscopy—All experiments were performed on a Leica DMI 6000B inverted epifluorescence microscope containing a motorized *xy* stage. Images were taken using a 14-bit dynamic range EM-CCD camera (C9100-12, Hamamatsu Photonics, Japan). For single cell trapping, an extension of the 1070-nm ytterbium fiber laser (YLD-5-LP-IPG laser) was used. A fluorescence light source (EL 6000, Leica Microsystems, Germany) was used together with a GFP filter cube (472/30-nm exciter, 520/35-nm emitter, and 495LP dichroic mirror, Semrock IDEX Corp.) and an mCherry filter cube (560/40-nm exciter, 630/75-nm emitter, and 585LP dichroic mirror, ET-TexRed, Chroma). The exposure times used were 27, 150, and 300 ms for the transmission, mCherry and GFP states, respectively.

Cell Imaging—Seven images with an axial distance of 0.8 μm were acquired in transmission and fluorescent light, respectively. The acquisition time of these images at each time point was ~30 s. Images were acquired at different time points (at 30 s before the shift, at the shift, at 60 s, every 60 s for 420 s, every 120 s for 360 s, and every 180 s for 360 s after the shift), generating an overall experiment time of 20 min. The transmission light images were used to calculate the cell size and contour by using the CellStat software. The fluorescent image data were used to obtain the nuclear size and localization (mCherry signal) as well as the dynamics of Mig1 localization (GFP signal).

Data Analysis—Image analysis and processing were performed using the custom-made CellStress software (30), which generates quantitative fluorescent intensity data in different cell compartments. The CellStress software detects the nuclei from the mCherry images and measures the GFP fluorescence intensity within the entire nuclear area as well as within the whole cell (using cell contour data extracted from CellStat) (31). Fluorescent intensity data are presented as the ratio of the GFP intensity in the entire nucleus relative to the intensity in the whole cytosol over time. 24–78 cells were analyzed at each glucose concentration.

Western Blot Analysis—To determine the phosphorylation status of Mig1, a 100-ml culture of strain YSH2361 (*MATa mig1Δ::LEU2*, W303–1A background) was transformed with the centromeric plasmid p*MIG1-HA* (32) and grown to mid-log phase in yeast nitrogen base medium, 4% glucose, lacking histidine. 7 ml of the culture were harvested, whereas the remaining culture was diluted to a final glucose concentration of 1%. The glucose concentration in the medium was verified by using the D-glucose/D-fructose kit (Roche) according to the protocol of the manufacturer. Samples were taken at the indicated time points (Fig. 5*A*), and cells were harvested by filtration and immediately frozen in liquid nitrogen. The following procedure has been adapted from Ye *et al.* (33). 2 ml of 2M NaOH was added, cells were vortexed until they were completely resuspended from the filters, and incubated for a couple of minutes at room temperature. Filters were removed, and 2 ml of 50% trichloroacetic acid was added. The samples were vortexed and centrifuged at maximal speed. The pellets were washed with 1.4 ml of 1M Tris-HCl (pH 7.5) resuspended in 250 μl of 1× SDS sample buffer (62.5mM Tris-HCl (pH 6.8), 3% SDS, 10% glycerol, 5% β-mercaptoethanol, and 0.004% bromphenol blue) and boiled for 5min at 100°C. 50 μg of proteins was separated by SDS-PAGE using 7.5% precast polyacrylamide gel (Bio-Rad) and analyzed by immunoblotting using mouse anti-HA (1:2000) antibody (Santa Cruz Biotechnology) and a secondary (1:15,000) horseradish peroxidase-conjugated anti-mouse IgG antibody (Promega).

For Snf1 phosphorylation, a 100-ml culture of strain YSH1701 (*MATa snf1Δ::KanMX*, W303–1A background) transformed with the centromeric plasmid p*SNF1-HA* (34) was grown until mid-log phase in yeast nitrogen base, 4% glucose, lacking uracil. 7 ml of the culture was harvested, and the rest of the culture was diluted to ensure a final glucose concentration of 1%. Samples were taken at the indicated time points (Fig. 5*B*). Protein extraction was performed as described for Mig1. For immunoprecipitation of Snf1, 120 μg of extracted proteins was resolved on an SDS-7.5% precast polyacrylamide gel and detected by either rabbit anti-Thr^{172} or rabbit anti-Thr^{210} (1:1000) together with mouse anti-HA (1:2000) antibodies. The primary antibodies were visualized simultaneously with goat (LI-COR Biosciences) anti-mouse IRDye-800CW (1:15000) and goat anti-rabbit IRDye-680CW (1:15000). Membranes were scanned with an infrared imager (Odyssey, LI-COR Biosciences) using both 700- and 800-nm channels simultaneously.

Photobleaching Experiments—The kinetics of Mig1-GFP nuclear-cytoplasmic movements was monitored using fluorescence recovery after photobleaching (FRAP). The FRAP experiments were performed using an inverted LSM 700 confocal microscope (Carl Zeiss, Germany). Nrd1-mCherry was used as a nuclear marker to define the nuclear bleach region. The GFP (excited at 488 nm and emission detected below 555 nm) and mCherry (excited at 555 nm and emission detected above 575 nm) fluorescence signals were imaged simultaneously using a

Plan-Apochromat ×63/1.40 oil objective, a zoom factor of 6, and a pinhole setting of 1 Airy Unit (AU). In addition, a simultaneous transmission channel was acquired to visualize the cell morphology and the focus plane. The FRAP time series consisted of a total of 100 scan cycles with a photobleaching event after five prebleach scans. The pixel resolution was 256 × 256, and the pixel dwell time was 1.27 μs (bidirectional scanning), giving a frame time of 97.75 ms. 22- 29 cells were averaged for each condition, *i.e.* 4, 1, and 0% glucose.

To investigate the kinetics of the rate of Mig1-GFP nuclear exit, fluorescence loss in photobleaching (FLIP) was applied using the same microscope setup as described above. The FLIP time series consisted of a total of 500 scan cycles, starting with five prebleach scans and then a photobleaching event before each following image. Bleaching was done in a circular region of interest with a radius of 5 pixels in the cytoplasm of the selected cell. 13–24 cells were averaged for each condition, *i.e.* 4, 1, and 0% glucose.

In each FRAP and FLIP measurement, one cell was chosen for the bleach experiment, whereas the other cells in the same field of view were used as control regions for bleach correction. The fitting of the recovery curves, the fitting of the loss curves, and the averaging of single cell data were done in MATLAB (The MathWorks, Inc.).

RESULTS

Mig1 Responds Rapidly and Repeatedly to Changes in Glucose Concentration—We first determined how quickly the Snf1-Mig1 system responds to changes in glucose concentration at the level of Mig1 nuclear shuttling and whether the system responds to repeated changes. Our imaging setup coupled to cell arrays and microfluidic control of the cell environment allows changing the environment within less than 2 s. Cells were pregrown in 4% glucose and arranged in cell arrays in the microfluidic device. In this experiment, we changed the conditions between 4 and 0.1% glucose every 600 s, starting with the higher glucose level. Nuclear Mig1 was monitored every 30 s and represented as the ratio of the mean fluorescence intensity in the nucleus relative to the intensity of the whole cytosol. Cells responded rapidly to the glucose shift. Within the time frame of the first measurement, the response was essentially complete (Fig. 2). Between shifts, cells showed minor fluctuations in the nuclear/cytosolic Mig1 proportion and appeared to stably maintain the new state. Upon the second shift to low glucose, it appears that cells responded somewhat more slowly. The decrease of Mig1 intensity occurring after 1800 s can be explained by GFP photobleaching and autofluorescence (35). Taken together, it appears that the Snf1-Mig1 system responds in a subminute time scale to changes in glucose concentration, maintains the state between shifts, and has the capacity to respond to repeated changes, albeit slower and with lower amplitude. These observations are in good agreement with data obtained using plasmid-borne, overexpressed Mig1-GFP employing up to five cycles and different intervals between shifts (35).

Mig1 Enters the Nucleus in Response to Very Low Amounts of Glucose—We moved on to determine the threshold glucose concentration that would trigger nuclear accumulation of Mig1 in derepressed yeast cells (cells adapted to absence of glucose) and to study the behavior of the signaling system around that threshold. Cells were pregrown in 3% ethanol as a carbon source and arranged in arrays in the microfluidic device. As a control, we switched the flow between two channels that contained medium lacking glucose. As expected, Mig1 did not change its localization (Fig. 3*A*). Cells showed a very similar response to glucose over a wide range of glucose concentrations, *i.e.* from 4% down to 0.05%. This concentration is significantly lower than that required to establish glucose repression of most yeast genes (see "Discussion"). Only when we shifted to a glucose concentration of lower than 0.05% did the response profile change. The amplitude of the response was lower, in a fraction of the cells the response also appeared to be slower, and not all cells responded. However, even at the lowest concentration employed, 0.005% glucose, it appeared that many cells moved a fraction of Mig1 to the nucleus. At this concentration, Mig1 translocation is clearly delayed (level-off time at 280 s compared with 150–200 s), and its amplitude is significantly lower compared with shifts to higher glucose concentrations. The coefficient of variation for each time point was approximately the same for most of the concentrations, with the 0.05% glucose experiment showing the lowest cell-to-cell variation (Fig. 3, *A* and *B*).

Mig1 Moves Transiently to the Cytoplasm When Shifted to Intermediate Glucose Levels—We then performed a series of experiments where cells were shifted from 4% glucose to different lower concentrations of glucose (Fig. 4). As a control, we changed to a flow channel with the same glucose concentration. As expected, we did not observe any response. Also, when cells were shifted to 2% glucose, Mig1 remained nuclear. However, when cells were shifted from 4% glucose to 1.5, 1.0, and 0.5% glucose, concentrations that still mediate glucose repression of Mig1 target genes (see "Discussion"), an unexpected behavior was observed. Mig1 was moved transiently to the cytosol but then moved back into the nucleus. The period of transient cytosolic residence increased with lower glucose levels. When cells were shifted to glucose levels of 0.2% or lower, Mig1 remained cytosolic during the course of the experiment. As in the glucose upshift experiments, cells responded rapidly, and Mig1 had almost completely moved to the cytosol at the time of the first measurement, *i.e.* 60 s.

Mig1 and Snf1 Phosphorylation Correlate with the Mig1 Localization Status—To better understand the unexpected transient Mig1 nuclear exit when cells were shifted from high to intermediate glucose levels, we monitored Snf1 and Mig1 phosphorylation in extracts from a cell population following a shift from 4 to 1% glucose. In the presence of glucose, both Snf1 and Mig1 are unphosphorylated or phosphorylated poorly, whereas, at low glucose levels or in the absence of glucose, Snf1 becomes phosphorylated and subsequently phosphorylates Mig1. Following the shift to lower glucose levels, we observed that Snf1 becomes clearly phosphorylated within less than 60 s and remained phosphorylated for at least 420 s before the phosphorylation dropped again (Fig. 5, *A* and *B*). Fig. 5*A* shows a spline interpolation of the Western blot quantifications of five independent experiments and illustrates that the trend in the Snf1 phosphorylation pattern is highly reproducible. Although Snf1 phosphorylation was

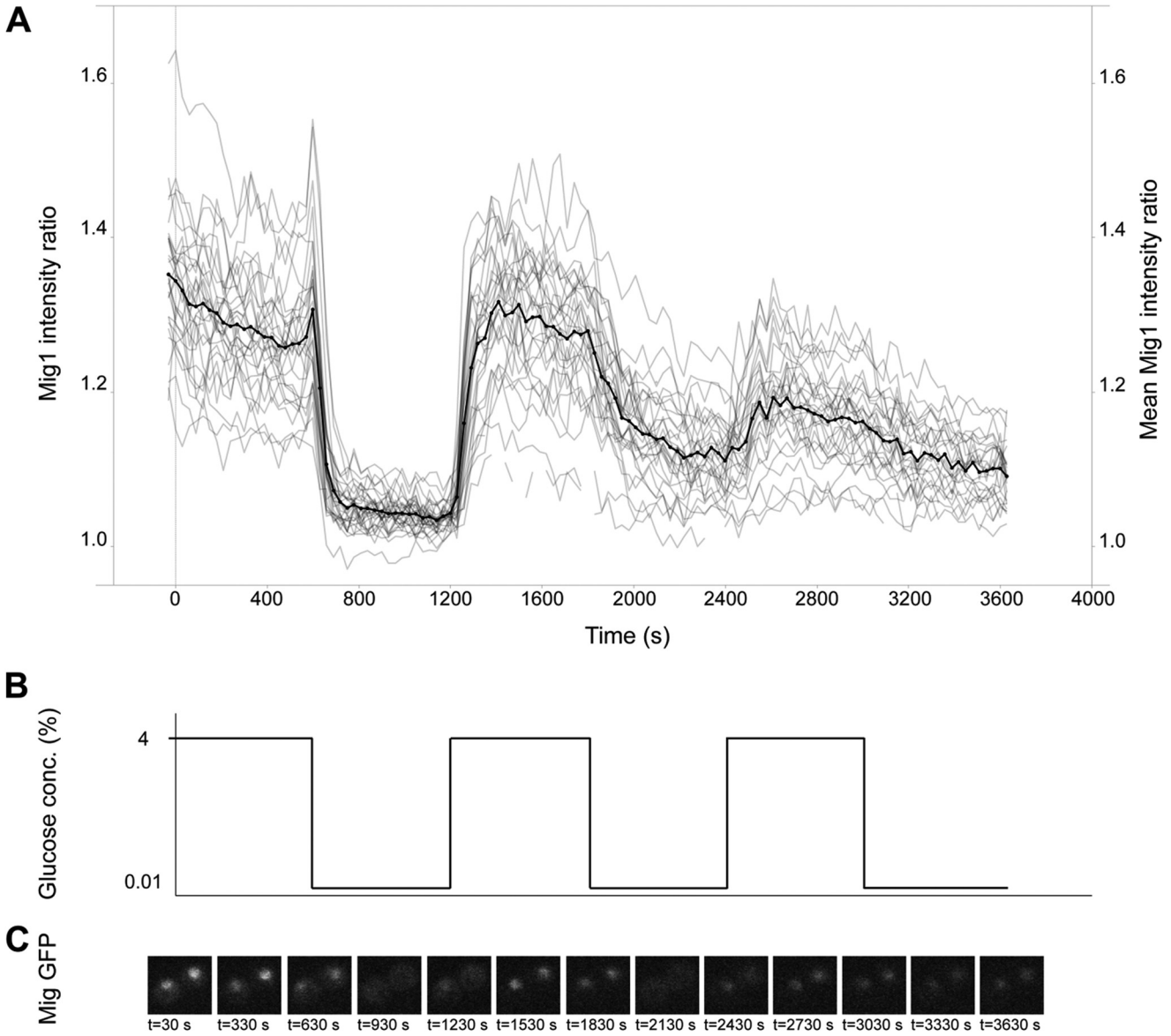

FIGURE 2. **Single cell data of Mig1 nuclear-cytoplasmic shuttling upon repetitive environmental changes.** *A*, ratio of the mean Mig1-GFP intensity in the nucleus relative to the whole cell obtained from 34 cells plotted over time. Traces for all cells as well as the average are shown. Cells were grown in 4% glucose until mid-log phase and then exposed to three cycles of repeated shifts between 4 and 0.1% glucose. The new conditions were established within 2 s. Each shift lasted for 600 s, resulting in a 3600-s experiment. Images were taken 30 s before the shift, at the shift, and every 60 s after the shift. *B*, glucose shift regime. *conc.*, concentration. *C*, images of the same two cells at different times of the experiment.

analyzed using an anti-phospho-Snf1-specific antibody, the phosphorylation status of Mig1 is monitored using band shifts, and the pattern is complicated by the fact that Mig1 is phosphorylated by Snf1 on multiple sites (21). The phosphorylation status of Mig1 also appears to change in the time window of 60–350 s after the glucose shift, with the strongest change between 100 and 160 s (Fig. 5*C*), which is roughly consistent with Mig1 localization dynamics. However, the Mig1 phosphorylation shift was not as pronounced as that in ethanol medium. Taken together, it appears that, following a shift from 4 to 1% glucose, Snf1 and Mig1 become transiently phosphorylated, consistent with the transient cytosolic accumulation of Mig1.

Mig1 Moves between Cytosol and Nucleus in the Presence and Absence of Glucose—To investigate the kinetic properties of Mig1 nuclear-cytoplasmic shuttling, we employed two different bleaching techniques, FRAP and FLIP. Experiments were carried out with cells expressing Mig1-GFP and Nrd1-mCherry, employing concentrations of 4, 1, and 0% glucose (but 3% ethanol as a carbon source instead). FRAP was performed by taking a time series of images where Mig1-GFP was bleached in the entire nucleus and the fluorescence recovery in this region was monitored. The FRAP recovery curves, *i.e.* the mean intensity in the nucleus as a function of time where the intensity after bleaching was set to 0, are shown in Fig. 6*A*. The fluorescence intensities were normalized with respect to the final recovered intensities to emphasize the time dependence of the process because the level of the final recovered intensity was much lower in the presence of glucose compared with that in the absence of glucose (not shown). This difference probably reflects the fact that, in the presence of glucose, most of the Mig1-GFP resides in the

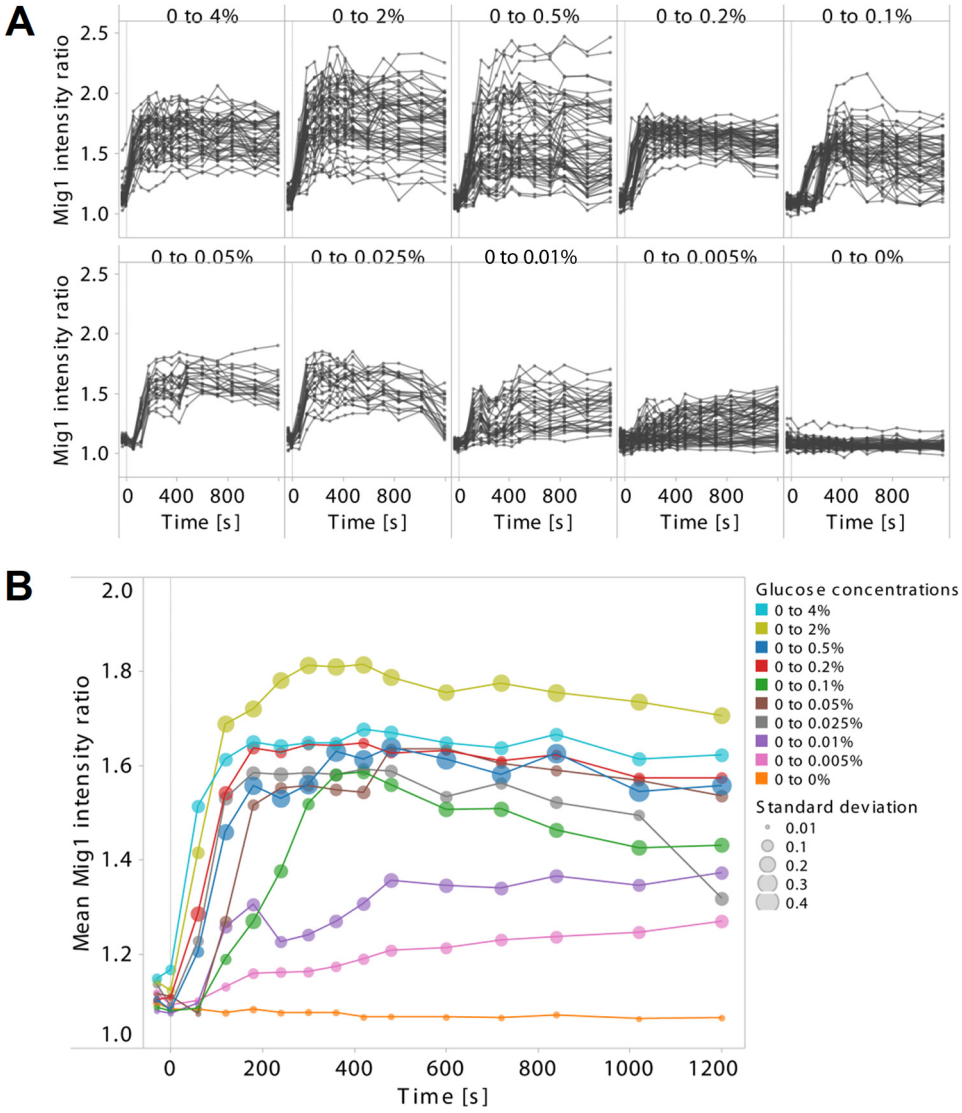

FIGURE 3. **Mig1 nuclear accumulation following a glucose upshift over time.** *A*, ratio of the mean Mig1-GFP intensity in the nucleus relative to the whole cell obtained from 24–64 single cells plotted over time. Cells were grown in 3% ethanol until mid-log phase, arrayed in the microfluidic device, kept in the same medium, and then shifted to glucose at a final concentration of 4, 2, 0.5, 0.2, 0.1, 0.05, 0.025, 0.01, 0.005, or 0%. The microfluidic flow was shifted at time 0 s, and images were taken 30 s before the shift, at the shift, at 30 s, every 60 s for 420 s, every 120 s for 360 s, and every 180 s for 360 s after the shift. *B*, mean of the Mig1-GFP intensity ratio for all cells shown in *A*. Glucose concentrations are represented with different colors, and the size of the *circles* represents mean ± S.D.

nucleus, and, therefore, a major fraction of Mig1-GFP is bleached and cannot contribute to the recovery. However, more importantly, the nuclear intensity showed recovery under all conditions tested, with a similar recovery rate for the two glucose concentrations and a slightly faster recovery in the absence of glucose. In the absence of glucose, the intensity already reached its final value at 3–4 s, whereas, in the presence of glucose, the intensity was still not fully recovered at the end of the measurements (9 s, Fig. 6*A*). We tried fitting the recovery curves with a single exponential function, but because this approach did not result in an acceptable representation of the data, we considered a double exponential fit. The double exponentials resulted in good-quality fits (Fig. 6*B* shows an example for the 4% glucose case), which would indicate that there is more than one pathway involved in Mig1 shuttling. The average values from the double exponential fits of the single cell data (see Fig. 7*A*–*C*) indicate that there might be two contributing factors for the overall faster recovery in the absence of glucose. The fast fraction (Fig. 7*C*) appears to decrease with increasing glucose levels, and the half-time of the slow fraction (Fig. 7*B*) appears to be shorter in the absence of glucose. The half-time of the fast fraction (Fig. 7*A*), on the other hand, seems to be longer in the absence of glucose. However, a double-exponential fit has more degrees of freedom than a single-exponential fit and, there is a large cell-to-cell variability for all conditions (see Fig. 6*C* for 4% glucose which precludes drawing firm conclusions from the recovery times or from fast/slow fractions. However, we believe that it is reasonable to conclude that Mig1 shuttles between the cytosol and nucleus under all conditions and that, to explain the data, at least two contributing pathway components need to be considered.

Employing FLIP, the time series consisted of repetitive bleaching in the cytoplasm, whereas fluorescence loss was monitored in the nuclear region (Fig. 6*D*). The fluorescence

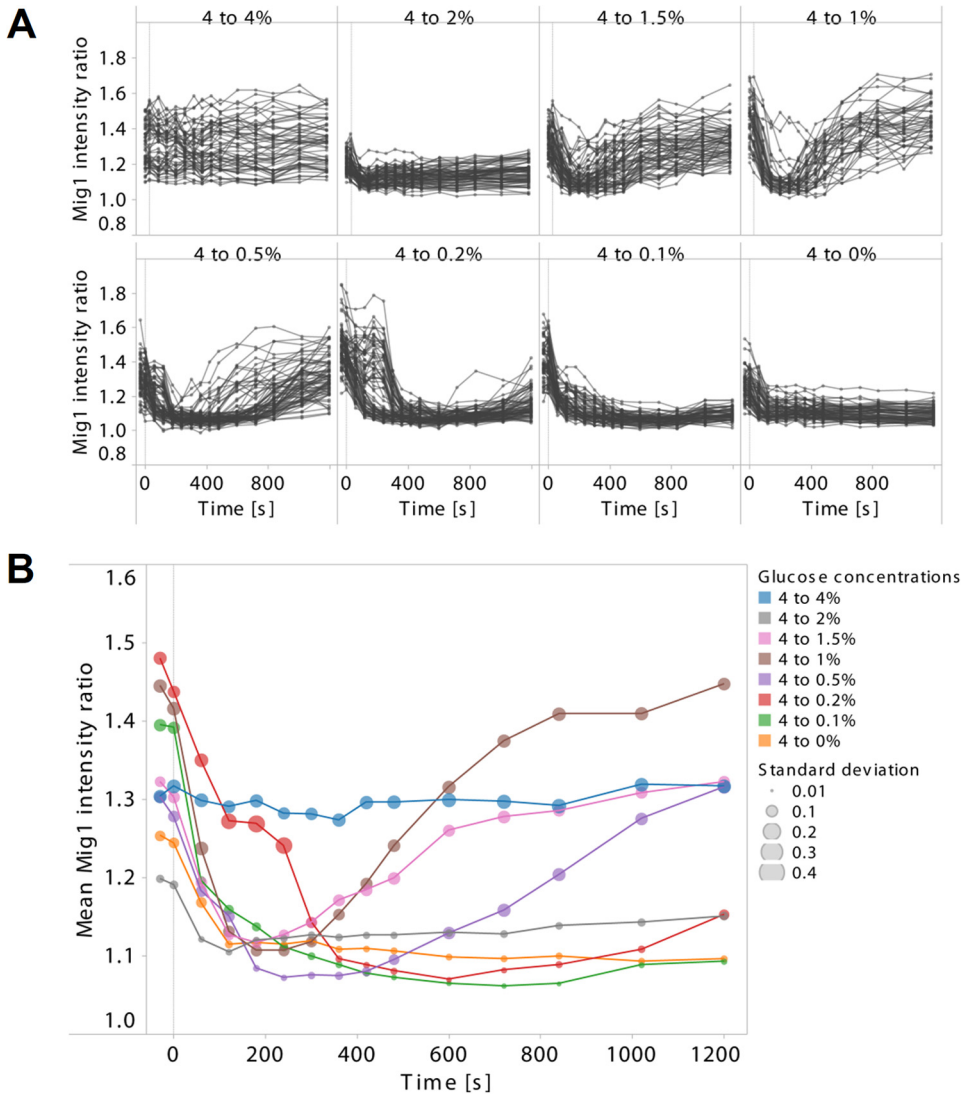

FIGURE 4. **Mig1 nuclear exit following a glucose downshift over time.** *A*, ratio of the mean Mig1-GFP intensity in the nucleus relative to the whole cell obtained from 45–78 individual single cells plotted over time. Cells were grown in 4% glucose until mid-log phase, arrayed in the microfluidic device, kept in the same medium, and then shifted to glucose at a final concentration of 4, 2, 1.5, 1, 0.5, 0.2, 0.1, or 0%. The microfluidic flow was shifted at time 0 s, and images were taken 30 s before the shift, at the shift, at 60 s, every 60 s for 420 s, every 120 s for 360 s, and every 180 s for 360 s after the shift. *B*, mean of the Mig1-GFP intensity ratio for all cells shown in *A*. Glucose concentrations are represented with different colors, and the size of the *circles* represents mean ± S.D. Initial values cannot be compared directly between experiments because different cell arrays where used and the equipment had to be readjusted between experiments.

intensity was corrected for photobleaching during imaging and normalized with respect to the initial intensity. The intensity in the nucleus diminished upon bleaching in the cytoplasm for all glucose concentrations, indicating that Mig1 exits the nucleus even in the presence of glucose. In the presence of glucose, the half-time of Mig1-GFP fluorescence loss is more than two times larger than in the absence of glucose (Fig. 7*D*). The notably slower exit rate of Mig1 from the nucleus in the presence of glucose is most likely one of the causes for net Mig1 nuclear accumulation.

DISCUSSION

In this study, we employed the cytoplasmic-nuclear movement of the Mig1 transcriptional repressor as a readout for the dynamics of the Snf1-Mig1 signaling in response to changes in extracellular glucose concentrations. In contrast with many well studied signaling systems, the Snf1-Mig1 pathway does not seem to be controlled by cell surface receptors. Rather, the stimuli that control the pathway are generated internally by central carbon and energy metabolism (11, 13). It has been demonstrated a long time ago that establishment of glucose repression (dephosphorylation of Snf1 and Mig1) requires the uptake of glucose and its phosphorylation but no further metabolism of glucose (36). Recent biochemical and structural studies of the SNF1 complex point to a central role of ATP, ADP, and AMP and, hence, metabolic signals in controlling SNF1 activity (13, 14, 37–40). Activation of SNF1, however, is not sufficient for mediating glucose derepression (41). Instead, there appears to be a second glucose-regulated step that enables active Snf1 to phosphorylate Mig1. SNF1 complex formation (42) or an involvement of the hexokinase enzyme in a regulatory role (43–45) are candidates for controlling such a step in

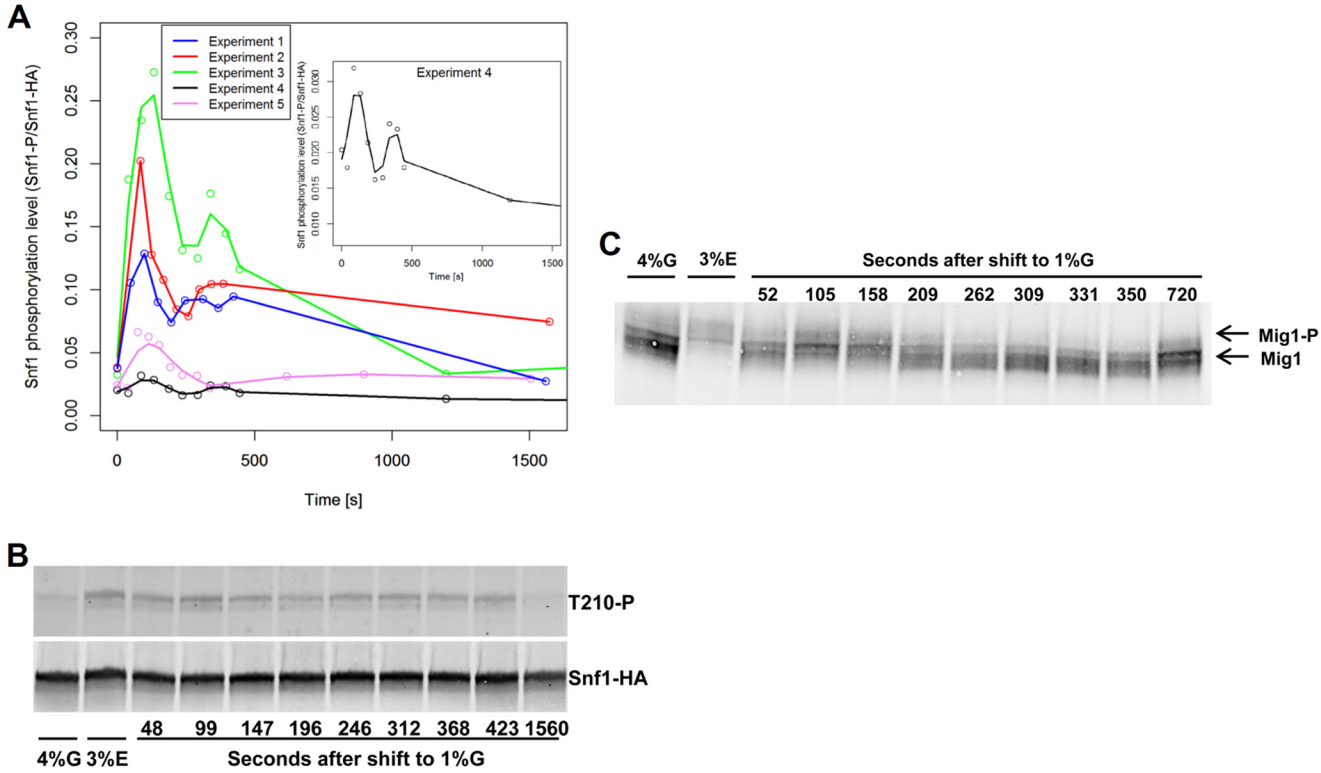

FIGURE 5. **Mig1 and Snf1 phosphorylation correlate with transient Mig1 relocalization.** *A*, the Snf1 phosphorylation status correlates with Mig1 subcellular localization. A *snf1*Δ mutant expressing p*SNF1*-HA was grown to mid-log phase in selective medium supplied with 4% glucose, and then the culture was diluted to 1% glucose. Samples were taken before and at the indicated time points after glucose shift and analyzed by immunoblotting using simultaneously anti-Thr^{172} and anti-HA antibodies. Western blot analysis data were quantified relative to total Snf1. Because different blots cannot be compared directly, a cubic spline interpolation of the ratio between phosphorylated Snf1 and total Snf1 over time from five independent experiments was performed in R-3.0.0. These data show that the overall trend in these five experiments is highly reproducible. *B*, representative blot of phosphorylated Snf1 relative to total Snf1 (*Experiment 2*, *red line* in *A*). *G*, glucose; *E*, ethanol. *C*, Mig1 phosphorylation correlates with its subcellular localization. Cells of a *mig1*Δ mutant expressing p*MIG1*-HA was treated as in *A*. Samples were taken before and at the indicated time points after glucose shift and analyzed by immunoblotting using anti-HA antibody.

response to a direct or indirect glucose stimulus. Taken together, the data of this study on the dynamic behavior of the Snf1-Mig1 system need to be interpreted with the connection between central metabolism and signaling in mind.

Mig1 migrates from the cytosol to the nucleus or vice versa following a shift in glucose concentration. Within 150 s, Mig1 localization reaches a new steady state. The time frame of the response is in agreement with that of changes of the levels of metabolites in the upper part of glycolysis following a glucose pulse, which typically increase within 30 s after glucose addition and then reach a new steady state or decline again (46, 47). Hence, it appears that the dynamics of the Snf1-Mig1 systems closely follows that of glycolytic metabolism. It further appears that the system remains sensitive to such changes even after repeated glucose shifts, as shown here and reported previously (35).

The glucose threshold concentrations for Mig1 subcellular movement differ strongly between glucose up- and downshifts. Cells adapted to the absence of glucose appear to be exquisitely sensitive to very low glucose concentrations and respond to even 0.005% glucose. Cells adapted to high glucose levels respond to a downshift from 4% to 1.5% by transient Mig1 nuclear export. Following a shift to 0.2% glucose Mig1 remains cytoplasmic during the course of the experiment (1200s). Previous work (26) reported that Mig1 is nuclear at 1% glucose and cytoplasmic at 0.005% glucose. The different glucose sensitivity of the system, depending on up- and downshift, suggests that the metabolism is adapted to the conditions so that glucose can be metabolized rapidly when it becomes available, whereas adjustments to a decline in the glucose concentration start before it is consumed completely. Such a metabolic adaptation probably provides signals to the Snf1-Mig1 system at different glucose thresholds, as observed here. The characteristics of the yeast sugar uptake system likely contribute to the observed effects (48–50). The high-affinity sugar uptake systems are down-regulated at high glucose concentrations, and, therefore, such cells have a reduced capacity to take up glucose at low concentrations, whereas high-affinity glucose transporters are expressed in cells adapted to the absence of glucose.

Mig1 represses genes whose expression displays very different glucose sensitivity. For instance, low glucose concentrations below 0.3% derepress and even strongly stimulate expression of the invertase gene *SUC2* (51, 52). On the other hand, genes encoding gluconeogenic enzymes are still repressed by much lower glucose concentrations (16). This suggests that subcellular localization of Mig1, although a suitable and convenient readout for Snf1-Mig1 pathway activity, is not a good indicator for Mig1-mediated gene expression effects and that additional mechanism adjust gene expression dependent on glucose levels. In fact, it has been reported that Mig1 persis-

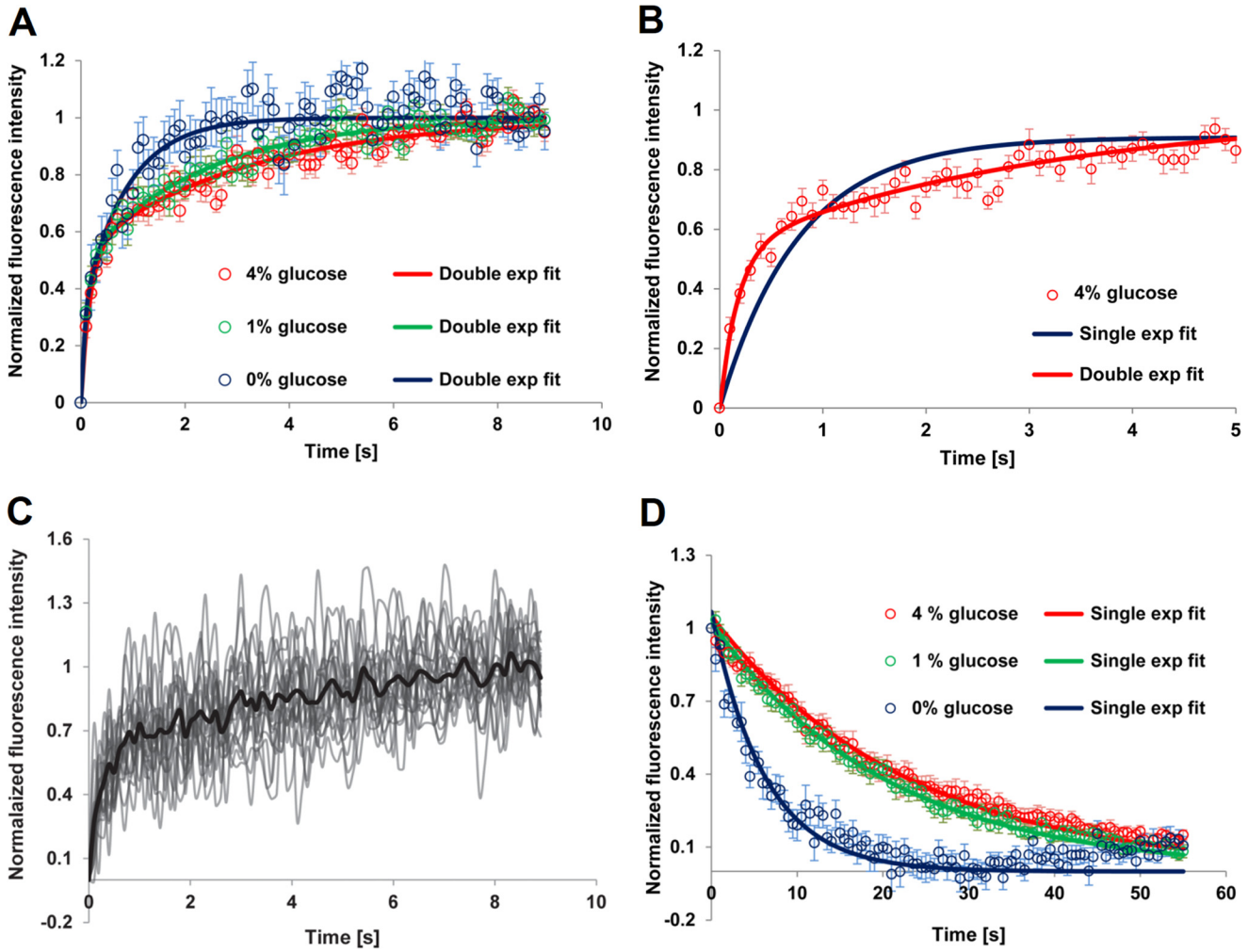

FIGURE 6. **Mig1 shuttles between the cytosol and nucleus under all conditions.** *A*, FRAP of Mig1-GFP under different glucose concentrations. Cells expressing Mig1-GFP and Nrd1-mCherry were grown to mid-log phase in 0, 1, or 4% glucose. Nuclei of individual cells were bleached, and the fluorescence recovery was recorded over time in those nuclei. The average of 20–25 cells normalized against the final recovered intensity for each glucose concentration (○) and the fit curve (*solid lines*) are represented over time. *B*, single *versus* double exponential fit. The average of 20 cells normalized against the final fluorescence recovery (○) together with the single (*blue line*) and double exponential (*red line*) fit curves plotted over time are shown. *C*, single cell FRAP curves from 20 cells grown in 4% glucose plotted over time. The mean of these cells is represented by a *bold line*. *D*, FLIP of Mig1-GFP under different glucose concentrations. Cells expressing Mig1-GFP and Nrd1-mCherry were grown to mid-log phase in 0, 1, or 4% glucose. In either case, a small region in the cytoplasm of individual cells was bleached, and the loss of fluorescence from the nucleus was recorded over time. The average of 13–24 cells normalized with respect to the initial intensity for each glucose concentration (○) and the fit curve (*solid line*) are represented over time. *Error bars* represent mean ± S.E.

tently occupies the *SUC2* and *GAL1* promoters (23). This suggests that, although a bulk of Mig1 shuttles between the cytosol and nucleus, a fraction of Mig1 remains nuclear under all conditions. This is consistent with our observation that Mig1 shuttles between the cytosol and nucleus under all conditions (see below).

The Mig1 nuclear accumulation profile changes when cells adapted to the absence of glucose are shifted to very low glucose levels.

1) The amplitude of the response, *i.e.* the fraction of Mig1 moving into the nucleus appears to drop across all cells. This suggests that the stimulus, which is generated by metabolism, follows a dose response at low glucose levels but is saturated at glucose levels above about 0.05% glucose (see also Refs. 53). This also shows that the Snf1-Mig1 system does not display an all-or-nothing behavior but, rather, displays a graded response characteristic at single cell level upon exposure to low glucose concentrations.

2) The response is delayed compared with shifts to higher glucose levels. At the lowest glucose concentrations tested here, the fraction of nuclear Mig1 only increases slowly, whereas, at higher glucose concentration, the response is maximal within less than 1 min. This suggests that, at low glucose levels, the metabolic adaptation controlling Snf1-Mig1 occurs gradually, whereas, at a higher glucose level, a new steady state is reached far more rapidly.

3) The cell variability appears to increase, and an increasing fraction of cells does not appear to respond at all. Upon shifts to higher glucose levels, the response across cells is far more uniform, at least with respect to its overall shape. The cell-to-cell variability may reflect already existing differences between cells with respect to expression of sugar transporters or metabolic enzymes, although all of those components are commonly highly expressed, and, hence, stochastic differences may not be that pronounced. The observed variability may also reflect stochastic differences between the number of signaling compo-

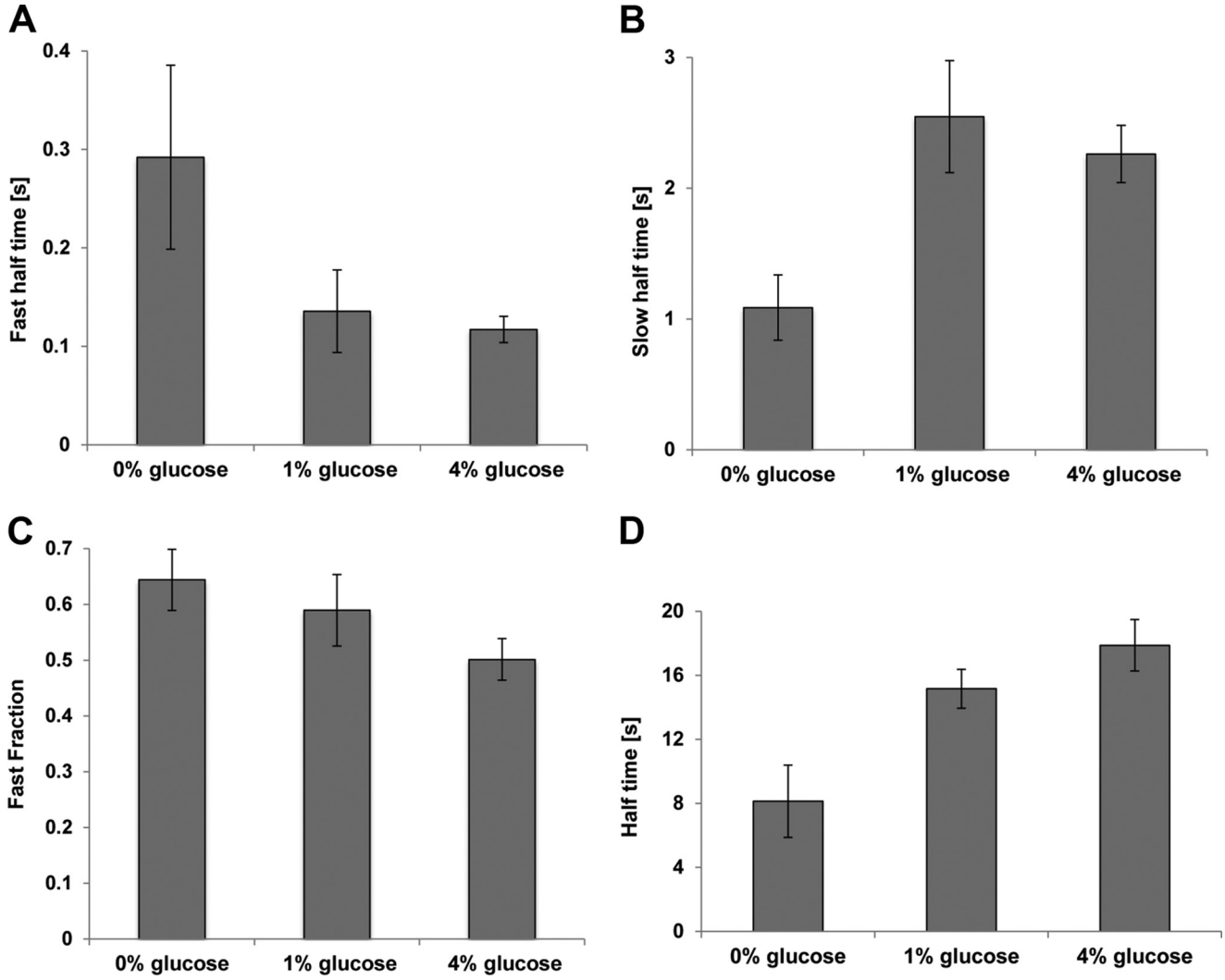

FIGURE 7. **Average results of the FRAP and FLIP fitting parameters.** The average of 20–25 cells of fast half-time (*A*), slow half-time (*B*), and fast fraction (*C*) of Mig1-GFP fluorescence recovery obtained from double exponential fits applied to 0, 1, and 4% glucose (Fig. 6*A*). *D*, average of 13–24 cells of half-time of Mig1-GFP fluorescence loss obtained from single exponential fits applied to 0, 1, and 4% glucose (Fig. 6*D*). *Error bars* represent mean ± S.E.

nents expressed in cells (8). For the population it may be advantageous that different cells respond differently under such conditions. The population as a whole would make use of available carbon sources optimally, whereas cells may differ in their individual prioritization of which carbon source is used. Environments that contain different carbon sources at low concentration may be common in nature.

Following a shift from high to intermediate glucose concentrations, Mig1 transiently leaves the nucleus, but, after a few minutes, it returns into the nucleus. This behavior is also reflected at the level of Snf1 and Mig1 phosphorylation, and, hence, appears to be a true transient change in signaling activity. The period of Mig1 cytoplasmic accumulation depends on the actual glucose concentration. This unexpected behavior suggests that the Snf1-Mig1 system responds not only to a change of the glucose level but also to the absolute glucose concentration. Apparently, the shift from *e.g.* 4 to 1% glucose is first perceived by central metabolism as absence of glucose, but the metabolism then rapidly adapts to the new condition, and the metabolic signals controlling Snf1-Mig1 are returned to a "normal" high glucose state. The period of the transient Mig1 cytoplasmic accumulation is too short to be explained by a gene expression response as a basis for the apparent adaptation. Rather, it appears that the activity of the sugar uptake systems or of metabolic enzymes is adjusted in some way. We are not aware of any studies that followed yeast glycolytic metabolism under these conditions.

Two different types of bleaching experiments were used to study the nuclear import and export kinetics of Mig1, and the data suggest that Mig1 shuttles between the cytosol and nucleus under all conditions, although with different rates. The data of the bleaching experiments also provide hints to the underlying mechanisms.

Although the FLIP dynamics were well described by single exponential functions, the recovery of Mig1 in response to nuclear bleaching required the sum of two exponentials to achieve a good fit. Although there typically are many different system configurations that can exhibit a certain behavior, it is often instructive to study minimal examples of those behaviors. Four simple dynamic system motifs, two of which display single exponential behavior and two of which display double exponential behavior, are shown in Fig. 8, *A* and *B*, respectively. The

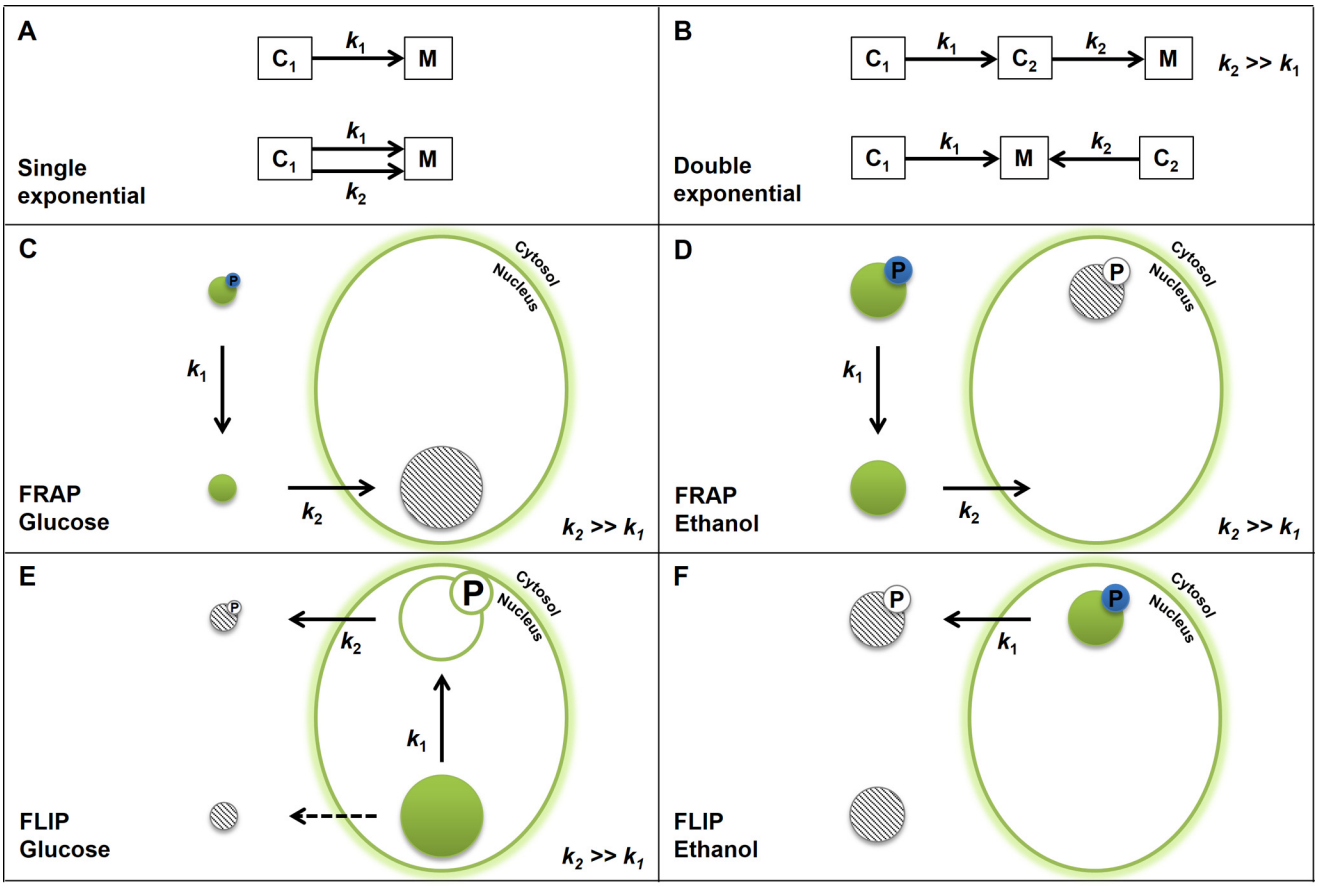

FIGURE 8. **Interpretation of FRAP and FLIP data.** *A*, and *B*, simple dynamic systems displaying either single or double exponential behavior. All reactions are assumed to have first-order kinetics. *C–F*, schematic of the pools of phosphorylated and unphosphorylated cytosolic and nuclear Mig1. The size of the *circles* illustrates the pool size at the start of each experiment. Pools affected by photobleaching at the start of an experiment are indicated by a *black and white diagonal pattern*, and phosphorylated pools are indicated with a small *sphere* with the letter *P* in the *top right corner*. All reactions are assumed to have first-order kinetics. *C*, FRAP for glucose-grown cells. After bleaching of nuclear Mig1, we first observe the rapid nuclear entry of unphosphorylated cytosolic Mig1, followed by relocalization of cytosolic phosphorylated Mig1 via a slower dephosphorylation step. This mechanism results in double exponential dynamics of the measured recovery of nuclear Mig1. *D*, FRAP for ethanol-grown cells. This is similar to the repressing (glucose) scenario but with different initial pool sizes. In this case, there is a relatively large amount of cytosolic Mig1. *E*, FLIP for glucose-grown cells. Nuclear unphosphoylated Mig1 is relocated to the cytosol via the initially empty pool of nuclear phosphorylated Mig1 (○). If the pool of nuclear phosphorylated Mig1 is initially empty and if the phosphorylation is significantly slower than the export reaction, a single exponential behavior is observed with a time constant that is larger compared with the derepressing scenario (as observed). Alternatively, the nuclear unphosphorylated Mig1 is directly exported to the cytosol (*dashed reaction*), also rendering single exponential behavior. *F*, FLIP for ethanol-grown cells. Nuclear Mig1 is assumed to be predominantly phosphorylated and is exported to the cytosol, resulting in single exponential dynamics.

variables C_1, C_2, and M denote the concentrations of some entities (whose identity depends on the context), where M is the only entity being measured. The first mechanism in Fig. 8*A* results in the solution $M(t) = M(0) + C_1(0)(1 - e^{-k1t})$ and the second one in $M(t) = M(0) + C_1(0)(1 - e^{-(k1 + k2)t})$, both consisting of a single exponential function. If $k_2 \gg k_1$, the first mechanism in Fig. 8*B* has the approximate solution $M(t) = M(0) + C_1(0)(1 - e^{-k1t}) + C_2(0)(1 - e^{-k2t})$, thus involving the sum of two exponentials. This is also the exact solution for the second mechanism.

As pointed out, the nuclear fluorescence recovery for glucose-grown cells showed a distinct double exponential behavior. On the basis of the dynamics of the mechanisms (Fig. 8*A*), neither one nor several parallel, first-order kinetic process(es) can explain this observation. However, the first mechanism in Fig. 8*B* could explain the good fit of the double exponential. One pool of Mig1 is first rapidly imported into the nucleus and is then followed by a slower conversion of a second pool into the first pool, which is then also imported rapidly. Because it is believed that only unphosphorylated Mig1 is imported into the nucleus (21, 26), it likely corresponds to the rapidly imported fraction of Mig1. The slower fraction, on the other hand, might be phosphorylated Mig1 that first needs to be dephosphorylated before being imported to the nucleus (Fig. 8*C*).

When the FRAP experiment was performed with ethanol-grown cells, the double exponential behavior model also resulted in a very good fit (Fig. 8*D*). This scenario differs from that of Fig. 8*C* only in that the proportion of cytoplasmic Mig1 is expected to be larger and that Mig1 in the nucleus before bleaching is assumed to be predominantly phosphorylated.

Although the double exponential dynamics of the FRAP experiments can be explained by the first mechanism of Fig. 8*B* (two consecutive conversions), the second mechanism cannot be completely ruled out. It would be possible to observe a double exponential behavior provided that, in addition to a fast import of unphosphorylated Mig1, there would be a direct, but slower, import of phosphorylated Mig1. This, however, is contradictory to present experimen-

tal evidence. It would also require that there is no equilibration between the two forms of Mig1 at the given time scale. Taken together, and considering that Mig1 is likely dephosphorylated in the cytosol, the scenarios depicted in Fig. 8, *C* and *D*, appear more probable.

Single exponentials fits were sufficient to describe the FLIP dynamics. In glucose-grown cells, one expects the majority of Mig1 to be unphosphorylated and located in the nucleus. Even though Snf1 should be largely inactive in the presence of glucose, residual activity could phosphorylate Mig1 so that it is rapidly exported from the nucleus. This two-step mechanism (Fig. 8*E*) is still compatible with a single exponential behavior as long as all, or most, Mig1 is in its unphosphorylated state. Alternatively, as illustrated by the dashed reaction, unphosphoylated Mig1 may be directly exported without the need of the Snf1 kinase activity, which, however, is in contradiction to the present view. At the same time, two independent experiments, one involving overexpression of the Mig1 exportin Msn5 and one involving mutation of Snf1 phosphorylation sites in Mig1, support this possibility (26).

In ethanol-grown cells, it is expected that nuclear Mig1 is phosphorylated. The export kinetics of this pool is observed following cytoplasmic bleaching (Fig. 8*F*). The export rate is expected to be faster than that of both routes discussed for repressing conditions. This is also what was observed.

The reasoning outlined above is on the basis of the assumption of first-order kinetics for all reactions. However, the observed double exponential behavior could, in principle, have emerged from a single transport reaction with higher-order kinetics involving a strong concavity, producing apparent first-order rate constants that are larger for large concentrations of the substrate. This would indicate highly cooperative effects of Mig1 during intercompartment transport, which is speculative without additional evidence. Rather, it would appear more plausible that the transport process involved shows saturable, convex kinetics (*i.e.* Michaelis-Menten). This scenario would give even more support to the suggestion that our observations in certain cases reflect other reactions preceding the actual transport step. Thus, the assumption of first-order kinetics is not a significant limitation for the analysis.

Taken together, the data presented here show that Snf1-Mig1 is controlled in a highly dynamic fashion. Although Mig1 appears to be predominantly nuclear in the presence of glucose and cytosolic in its absence, Mig1, in fact, shuttles between the cytosol and nucleus under all conditions, albeit with different rates. The system appears to respond differently to glucose up- and downshifts, and this behavior may reflect adaptations of sugar transport and glycolytic metabolism. Also, the ability to detect glucose concentration changes as well as absolute glucose levels may be due to stimuli generated by the central metabolism. The Snf1-Mig1 systems appears to be a remarkably flexible and sensitive signaling system tuned to rapidly and dynamically adjust gene expression programs, depending on the metabolic state. It also appears to enable cell variability at very low glucose levels, perhaps to ensure that the population as a whole makes optimal use of the available resources.

REFERENCES

1. Muzzey, D., Gómez-Uribe, C. A., Mettetal, J. T., and van Oudenaarden, A. (2009) A systems-level analysis of perfect adaptation in yeast osmoregulation. *Cell* **138,** 160–171
2. Pelet, S., Rudolf, F., Nadal-Ribelles, M., de Nadal, E., Posas, F., and Peter, M. (2011) Transient activation of the HOG MAPK pathway regulates bimodal gene expression. *Science* **332,** 732–735
3. Miermont, A., Waharte, F., Hu, S., McClean, M. N., Bottani, S., Léon, S., and Hersen, P. (2013) Severe osmotic compression triggers a slowdown of intracellular signaling, which can be explained by molecular crowding. *Proc. Natl. Acad. Sci. U.S.A.* **110,** 5725–5730
4. Geijer, C., Medrala-Klein, D., Petelenz-Kurdziel, E., Ericsson, A., Smedh, M., Andersson, M., Goksör, M., Nadal-Ribelles, M., Posas, F., Krantz, M., Nordlander, B., and Hohmann, S. (2013) Initiation of the transcriptional response to hyperosmotic shock correlates with the potential for volume recovery. *FEBS J.* **280,** 3854–3867
5. Babazadeh, R., Adiels, C. B., Smedh, M., Petelenz-Kurdziel, E., Goksör, M., and Hohmann, S. (2013) Osmostress-induced cell volume loss delays yeast hog1 signaling by limiting diffusion processes and by hog1-specific effects. *PLoS ONE* **8,** e80901
6. Cai, L., Dalal, C. K., and Elowitz, M. B. (2008) Frequency-modulated nuclear localization bursts coordinate gene regulation. *Nature* **455,** 485–490
7. Sunnåker, M., Zamora-Sillero, E., Dechant, R., Ludwig, C., Busetto, A. G., Wagner, A., and Stelling, J. (2013) Automatic generation of predictive dynamic models reveals nuclear phosphorylation as the key Msn2 control mechanism. *Sci. Signal.* **6,** ra41
8. Petrenko, N., Chereji, R. V., McClean, M. N., Morozov, A. V., and Broach, J. R. (2013) Noise and interlocking signaling pathways promote distinct transcription factor dynamics in response to different stresses. *Mol. Biol. Cell* **24,** 2045–2057
9. Hao, N., Budnik, B. A., Gunawardena, J., and O'Shea, E. K. (2013) Tunable signal processing through modular control of transcription factor translocation. *Science* **339,** 460–464
10. Wood, M. J., Storz, G., and Tjandra, N. (2004) Structural basis for redox regulation of Yap1 transcription factor localization. *Nature* **430,** 917–921
11. Ghillebert, R., Swinnen, E., Wen, J., Vandesteene, L., Ramon, M., Norga, K., Rolland, F., and Winderickx, J. (2011) The AMPK/SNF1/SnRK1 fuel gauge and energy regulator: structure, function and regulation. *FEBS J.* **278,** 3978–3990
12. Broach, J. R. (2012) Nutritional control of growth and development in yeast. *Genetics* **192,** 73–105
13. Hardie, D. G., Ross, F. A., and Hawley, S. A. (2012) AMPK: a nutrient and energy sensor that maintains energy homeostasis. *Nat. Rev. Mol. Cell Biol.* **13,** 251–262
14. Carling, D., Thornton, C., Woods, A., and Sanders, M. J. (2012) AMP-activated protein kinase: new regulation, new roles? *Biochem. J.* **445,** 11–27
15. Carling, D., Mayer, F. V., Sanders, M. J., and Gamblin, S. J. (2011) AMP-activated protein kinase: nature's energy sensor. *Nat. Chem. Biol.* **7,** 512–518
16. Schüller, H. J. (2003) Transcriptional control of nonfermentative metabolism in the yeast *Saccharomyces cerevisiae*. *Curr. Genet.* **43,** 139–160
17. Hedbacker, K., and Carlson, M. (2008) SNF1/AMPK pathways in yeast. *Front. Biosci.* **13,** 2408–2420
18. Wu, J., and Trumbly, R. J. (1998) Multiple regulatory proteins mediate repression and activation by interaction with the yeast Mig1 binding site. *Yeast* **14,** 985–1000
19. Treitel, M. A., Kuchin, S., and Carlson, M. (1998) Snf1 protein kinase regulates phosphorylation of the Mig1 repressor in *Saccharomyces cerevisiae*. *Mol. Cell. Biol.* **18,** 6273–6280
20. Treitel, M. A., and Carlson, M. (1995) Repression by SSN6-TUP1 is directed by MIG1, a repressor/activator protein. *Proc. Natl. Acad. Sci. U.S.A.* **92,** 3132–3136
21. Ostling, J., and Ronne, H. (1998) Negative control of the Mig1p repressor by Snf1p-dependent phosphorylation in the absence of glucose. *Eur. J. Biochem.* **252,** 162–168
22. Ostling, J., Carlberg, M., and Ronne, H. (1996) Functional domains in the

Mig1 repressor. *Mol. Cell. Biol.* **16,** 753–761
23. Papamichos-Chronakis, M., Gligoris, T., and Tzamarias, D. (2004) The Snf1 kinase controls glucose repression in yeast by modulating interactions between the Mig1 repressor and the Cyc8-Tup1 co-repressor. *EMBO Rep.* **5,** 368–372
24. Frolova, E., Johnston, M., and Majors, J. (1999) Binding of the glucose-dependent Mig1p repressor to the *GAL1* and *GAL4* promoters *in vivo*: regulation by glucose and chromatin structure. *Nucleic Acids Res.* **27,** 1350–1358
25. DeVit, M. J., and Johnston, M. (1999) The nuclear exportin Msn5 is required for nuclear export of the Mig1 glucose repressor of *Saccharomyces cerevisiae*. *Curr. Biol.* **9,** 1231–1241
26. De Vit, M. J., Waddle, J. A., and Johnston, M. (1997) Regulated nuclear translocation of the Mig1 glucose repressor. *Mol. Biol. Cell* **8,** 1603–1618
27. Eriksson, E., Sott, K., Lundqvist, F., Sveningsson, M., Scrimgeour, J., Hanstorp, D., Goksör, M., and Granéli, A. (2010) A microfluidic device for reversible environmental changes around single cells using optical tweezers for cell selection and positioning. *Lab Chip* **10,** 617–625
28. Gustavsson, A. K., van Niekerk, D. D., Adiels, C. B., du Preez, F. B., Goksör, M., and Snoep, J. L. (2012) Sustained glycolytic oscillations in individual isolated yeast cells. *FEBS J.* **279,** 2837–2847
29. Scrimgeour, J., Eriksson, E., and Goksör, M. (2007) Laser surgery and optical trapping in a laser scanning microscope. *Methods Cell Biol.* **82,** 629–646
30. Smedh, M., Beck, C., Sott, K., and Goksor, M. (2010) CellStress: open source image analysis program for single-cell analysis. Proc. SPIE 7762, *Optical Trapping and Optical Micromanipulation VII*, 77622N; doi:10.1117/12.860403
31. Kvarnström, M., Logg, K., Diez, A., Bodvard, K., and Käll, M. (2008) Image analysis algorithms for cell contour recognition in budding yeast. *Opt. Express* **16,** 12943–12957
32. Schmidt, M. C., and McCartney, R. R. (2000) β-Subunits of Snf1 kinase are required for kinase function and substrate definition. *EMBO J.* **19,** 4936–4943
33. Ye, T., Elbing, K., and Hohmann, S. (2008) The pathway by which the yeast protein kinase Snf1p controls acquisition of sodium tolerance is different from that mediating glucose regulation. *Microbiology* **154,** 2814–2826
34. McCartney, R. R., and Schmidt, M. C. (2001) Regulation of Snf1 kinase. Activation requires phosphorylation of threonine 210 by an upstream kinase as well as a distinct step mediated by the Snf4 subunit. *J. Biol. Chem.* **276,** 36460–36466
35. Frey, S., Sott, K., Smedh, M., Millat, T., Dahl, P., Wolkenhauer, O., and Goksör, M. (2011) A mathematical analysis of nuclear intensity dynamics for Mig1-GFP under consideration of bleaching effects and background noise in *Saccharomyces cerevisiae*. *Mol. Biosyst.* **7,** 215–223
36. Rose, M., Albig, W., and Entian, K. D. (1991) Glucose repression in *Saccharomyces cerevisiae* is directly associated with hexose phosphorylation by hexokinases PI and PII. *Eur. J. Biochem.* **199,** 511–518
37. Xiao, B., Sanders, M. J., Underwood, E., Heath, R., Mayer, F. V., Carmena, D., Jing, C., Walker, P. A., Eccleston, J. F., Haire, L. F., Saiu, P., Howell, S. A., Aasland, R., Martin, S. R., Carling, D., and Gamblin, S. J. (2011) Structure of mammalian AMPK and its regulation by ADP. *Nature* **472,** 230–233
38. Mayer, F. V., Heath, R., Underwood, E., Sanders, M. J., Carmena, D., McCartney, R. R., Leiper, F. C., Xiao, B., Jing, C., Walker, P. A., Haire, L. F., Ogrodowicz, R., Martin, S. R., Schmidt, M. C., Gamblin, S. J., and Carling, D. (2011) ADP regulates SNF1, the *Saccharomyces cerevisiae* homolog of AMP-activated protein kinase. *Cell Metab.* **14,** 707–714
39. Hardie, D. G., Carling, D., and Gamblin, S. J. (2011) AMP-activated protein kinase: also regulated by ADP? *Trends Biochem. Sci.* **36,** 470–477
40. Hardie, D. G. (2011) Signal transduction: How cells sense energy. *Nature* **472,** 176–177
41. García-Salcedo, R., Lubitz, T., Beltran, G., Elbing, K., Tian, Y., Frey, S., Wolkenhauer, O., Krantz, M., Klipp, E., and Hohmann, S. (2014) Glucose derepression by yeast AMP-activated protein kinase SNF1 is controlled via at least two independent steps. *FEBS J.*, in press, 10.1111/febs.12753
42. Chandrashekarappa, D. G., McCartney, R. R., and Schmidt, M. C. (2013) Ligand binding to the AMP-activated protein kinase active site mediates protection of the activation loop from dephosphorylation. *J. Biol. Chem.* **288,** 89–98
43. Ahuatzi, D., Riera, A., Peláez, R., Herrero, P., and Moreno, F. (2007) Hxk2 regulates the phosphorylation state of Mig1 and therefore its nucleocytoplasmic distribution. *J. Biol. Chem.* **282,** 4485–4493
44. Ahuatzi, D., Herrero, P., de la Cera, T., and Moreno, F. (2004) The glucose-regulated nuclear localization of hexokinase 2 in *Saccharomyces cerevisiae* is Mig1-dependent. *J. Biol. Chem.* **279,** 14440–14446
45. Herrero, P., Martínez-Campa, C., and Moreno, F. (1998) The hexokinase 2 protein participates in regulatory DNA-protein complexes necessary for glucose repression of the SUC2 gene in *Saccharomyces cerevisiae*. *FEBS Lett.* **434,** 71–76
46. Van Aelst, L., Hohmann, S., Bulaya, B., de Koning, W., Sierkstra, L., Neves, M. J., Luyten, K., Alijo, R., Ramos, J., and Coccetti, P. (1993) Molecular cloning of a gene involved in glucose sensing in the yeast *Saccharomyces cerevisiae*. *Mol. Microbiol.* **8,** 927–943
47. Neves, M. J., Hohmann, S., Bell, W., Dumortier, F., Luyten, K., Ramos, J., Cobbaert, P., de Koning, W., Kaneva, Z., and Thevelein, J. M. (1995) Control of glucose influx into glycolysis and pleiotropic effects studied in different isogenic sets of *Saccharomyces cerevisiae* mutants in trehalose biosynthesis. *Curr. Genet.* **27,** 110–122
48. Horák, J. (2013) Regulations of sugar transporters: insights from yeast. *Curr. Genet.* **59,** 1–31
49. Leandro, M. J., Fonseca, C., and Gonçalves, P. (2009) Hexose and pentose transport in ascomycetous yeasts: an overview. *FEMS Yeast Res.* **9,** 511–525
50. Gancedo, J. M. (2008) The early steps of glucose signalling in yeast. *FEMS Microbiol. Rev.* **32,** 673–704
51. Ozcan, S., Vallier, L. G., Flick, J. S., Carlson, M., and Johnston, M. (1997) Expression of the SUC2 gene of *Saccharomyces cerevisiae* is induced by low levels of glucose. *Yeast* **13,** 127–137
52. Meijer, M. M., Boonstra, J., Verkleij, A. J., and Verrips, C. T. (1998) Glucose repression in *Saccharomyces cerevisiae* is related to the glucose concentration rather than the glucose flux. *J. Biol. Chem.* **273,** 24102–24107
53. Yin, Z., Wilson, S., Hauser, N. C., Tournu, H., Hoheisel, J. D., and Brown, A. J. (2003) Glucose triggers different global responses in yeast, depending on the strength of the signal, and transiently stabilizes ribosomal protein mRNAs. *Mol. Microbiol.* **48,** 713–724